Nuclear Instruments and Methods in Physics Research A 1063 (2024) 169255

Contents lists available at ScienceDirect

Nuclear Inst. and Methods in Physics Research, A

journal homepage: www.elsevier.com/locate/nima

Full Length Article

Maxwell–Boltzmann-like neutron spectrum production for Maxwellian averaged cross sections measurements

Elizabeth Musacchio-González [a,b,*], Pierfrancesco Mastinu [a], Guido Martín-Hernández [c], Ignacio Porras [d], Lisa Centofante [a], Fernando Arias de Saavedra [d], Luca Maran [e,a], Alberto Ruzzon [a], Daniele Lideo [e,a]

[a] INFN - Laboratori Nazionali di Legnaro, Viale dell'Università 2, Legnaro, 35020, Padova, Italy
[b] UNIFE - Universitá degli Studi di Ferrara, Via Ludovico Ariosto 35, Ferrara, 44121, Ferrara, Italy
[c] Centro de Aplicaciones Tecnol'ogicas y Desarrollo Nuclear, Calle 30 No. 502, Playa, 11300, La Habana, Cuba
[d] Departamento de F'isica At'omica, Molecular y Nuclear, Facultad de Ciencias, Universidad de Granada, E.18071, Granada, Spain
[e] UNIPD - Università degli Studi di Padova, Via 8 Febbraio 2, Padova, 35122, Padova, Italy

ARTICLE INFO

Keywords:
MACS
Cross section
nTOF
Time-of-flight
Accelerator based neutron source

ABSTRACT

Over the years, Maxwellian Averaged Cross Sections (MACS) have been measured by neutron activation, providing a neutron energy spectrum resembling the one found inside the stars. Recently, a new method has been proposed to produce stellar spectra at different stellar temperatures (a Maxwell–Boltzmann neutron energy distribution), employing the ^{7}Li(p,n)^{7}Be reaction. The method is based on the idea of shaping the proton beam energy to shape the neutron beam spectrum. This method was applied to obtain a well-reproduced Maxwell–Boltzmann neutron spectrum (MBNS) at $kT = 28$ keV. An initial proton energy of 3170 keV and an aluminum foil as a proton energy shaper were employed. Differential angular neutron energy distributions from 0 to 90 degrees in 10° steps were measured to obtain the 0°–90° integrated neutron spectrum over a neutron flight path of 50 cm. This manuscript reports on the measurement results, confirming the method's capability, and suggests the approach for producing a high-quality MBNS at $kT = 28$ keV.

1. Introduction

In stellar models, the Maxwellian Averaged Cross Section (MACS) is frequently used to calculate the reaction rate in neutron capture processes. By definition, MACS is the reaction rate normalized by the most probable velocity of the Maxwell–Boltzmann distribution:

$$\mathrm{MACS} = \frac{\langle \sigma v \rangle}{v_T} = \frac{2}{\sqrt{\pi}} \frac{1}{(kT)^2} \int_0^\infty \sigma(E)\, E\, e^{-E/kT} dE, \tag{1}$$

where kT is the temperature of the stellar environment, and $\sigma(E)$ is the energy-dependent capture cross section.

For the s-process, MACS directly describes the reaction rate inside stars for a given temperature. Hence, it is essential to determine the MACS with the lowest possible uncertainty. A very accurate and direct MACS measurement, under certain conditions, can be performed by neutron activation analysis if it is used a neutron beam with the appropriate stellar spectrum. The value of the MACS for a particular isotope can be measured from the induced activity when irradiating a sample of the isotope with a stellar neutron field.

The neutron capture on a nucleus can be expressed as:

$$^{A}X + \mathrm{n} \rightarrow {}^{A+1}X^{*} \rightarrow {}^{A+1}X + \gamma, \tag{2}$$

If the produced nucleus ^{A+1}X is radioactive, it will decay emitting particles (e.g. γ, β^{-}). Both, gamma and beta emitters can be experimentally measured. There are always two phases in the activation technique: the irradiation of the sample and the detection of the particles emitted by the freshly produced isotope (^{A+1}X) after the neutron irradiation. The activation technique is achievable if the produced isotope is radioactive and if its half-life is in a time range suitable for the activity measurement.

In 1988, Ratynski and Käppeler (R&K) [1] published a MACS measurement using the activation method for the ^{197}Au(n,γ) reaction at $kT = 25$ keV, producing a quasi-stellar neutron spectrum via the ^{7}Li(p,n)^{7}Be reaction [2]. In recent years, Lederer et al. [3], Feinberg et al. [4], and Macías et al. [5] have performed experiments to validate the neutron spectrum obtained by R&K. In all these experiments, neutron energy spectra have been measured by the time-of-flight (TOF) technique. According to R&K, with proton energies of 1912 keV from

* Corresponding author at: INFN - Laboratori Nazionali di Legnaro, Viale dell'Università 2, Legnaro, 35020, Padova, Italy.
E-mail address: musacchio@lnl.infn.it (E. Musacchio-González).

https://doi.org/10.1016/j.nima.2024.169255
Received 14 December 2023; Received in revised form 2 March 2024; Accepted 14 March 2024
Available online 16 March 2024

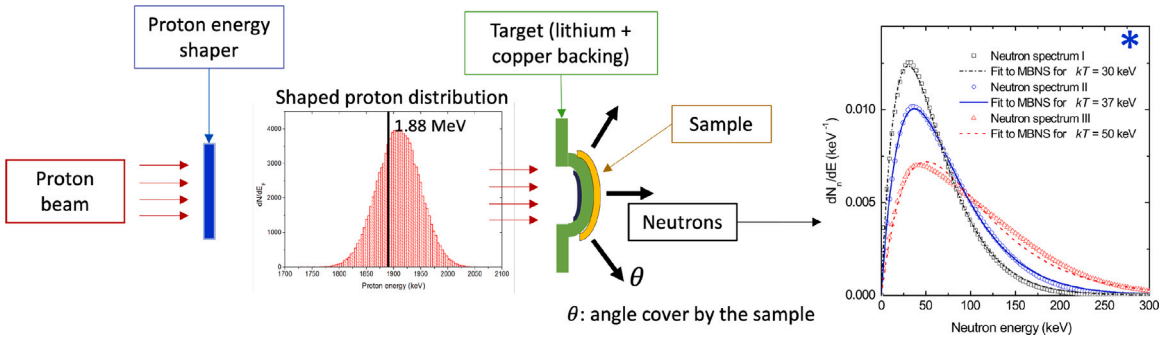

Fig. 1. Method to produce a Maxwell–Boltzmann neutron spectrum (MBNS), proposed by Mastinu et al. [6]. *This plot was reported by Martín-Hernández et al. [7].

the ^{7}Li(p,n)^{7}Be reaction, a good approximation to a 25 keV Maxwell–Boltzmann Neutron Spectrum (MBNS) is obtained. The measured spectrum has been used for a long campaign of MACS measurements using the activation method, producing high-quality data. However, there is a remarkable difference in shape between the experimental neutron spectrum obtained by R&K and the ideal stellar spectrum, particularly in the high-energy part of the spectrum. Due to the reaction kinematics, the observed neutron spectrum of R&K has an energy cutoff of around 110 keV. In contrast, the Maxwell–Boltzmann spectrum has a tail that theoretically extends to infinity. Because of these differences, a correction must be applied to obtain the MACS from experiments when a sample is irradiated with this field. The value of this correction and, even more, its uncertainty are difficult to determine since assumptions about the cross section to be measured have to be considered. Hence, the importance of having a high-quality MBNS. The main goal of this work is to produce and measure a neutron beam with a stellar spectrum in an accelerator based neutron source by shaping the proton beam energy.

2. The new proposed improvement

Mastinu et al. [6] proposed a possible solution to the problem of producing a high-quality Maxwell–Boltzmann neutron spectrum at $kT = 30$ keV. The method is based on the idea of shaping the proton beam energy distribution to tailor the neutron energy beam to the desired distribution. Among the many ways to shape the proton beam energy distribution, the simplest one relies on passing the beam through a thin foil placed before the neutron-producing target. A schematic representation of this method is shown in Fig. 1. A monochromatic proton beam passes through the proton energy shaper, producing a Gaussian-like proton energy distribution. The shaped beam impinges on a thick natural Li target producing a neutron field that will follow a Maxwell–Boltzmann distribution. By tuning the shaper foil thickness, the angular range subtended by the sample to be irradiated, and the proton energies, different thermal temperatures (kT) can be obtained [7].

The present work employed the same method to produce an MBNS with a thermal temperature of 30 keV. The foil (or proton energy shaper) and its thickness were studied to ensure this condition. The requirement that no neutrons were produced by the materials used in the foil was a crucial constraint in the proton energy shaper selection. This condition ensures that only neutrons from the ^{7}Li(p,n)^{7}Be reaction were generated and detected in the measurement. To this purpose, different materials and their isotopes were studied: carbon (C), aluminum (Al), titanium (Ti), copper (Cu), and lead (Pb). The proton energy threshold for neutron production, the value of the (p,n) cross section, the neutron yield, the gamma yield, and the stopping power were all considered for the analysis.

In 1999, Lee and Zhou [8] studied the kinematics and yield of the near-threshold ^{7}Li(p,n)^{7}Be reaction. In that work, the authors developed a method for computing angular distributions, energy spectra, and total yields of this reaction for energies near the reaction threshold using a compilation of data from Liskien and Paulsen [9]. Following the same procedure employed by Lee and Zhou, the authors of this work programmed a code, named TYpLi, to calculate the differential neutron yield. Using one degree and one keV interval, the double differential neutron yield is calculated for neutron emission polar angles in the range $0° \leq \theta \leq 90°$, neutron energies (E_n) from 0 keV to 600 keV, and proton energies (E_p) from 1.88 MeV to 2.28 MeV. Considering the Gaussian-like proton distribution with mean proton energy (E_m), the generated neutron spectrum has the form:

$$\frac{\mathrm{d}Y}{\mathrm{d}E_\mathrm{n}}\left(E_\mathrm{n}\right) = 2\pi\frac{1}{\sigma\sqrt{2\pi}}\int_{\theta_\mathrm{min}}^{\theta_\mathrm{max}}\int_{E_m-4\sigma}^{E_m+4\sigma} e^{-\frac{(E_p-E_m)^2}{2\sigma^2}} \times \frac{\mathrm{d}^2Y}{\mathrm{d}\Omega\mathrm{d}E_\mathrm{n}}\left(\theta, E_\mathrm{n}\right)\sin\theta\ \mathrm{d}\theta\ \mathrm{d}E_p, \tag{3}$$

where θ_{min} and θ_{max} are the minimum and the maximum neutron angle for the integration, and σ is the standard deviation of the Gaussian distribution. The E_m, FWHM $= \sigma\ (2\sqrt{2\ln 2})$, θ_{min}, and θ_{max} are the input parameters for the TYpLi code. The theoretical neutron energy spectrum, calculated from Eq. (3), is the output of the TYpLi code.

To properly dimension the proton energy shaper, calculations were performed using the Stopping and Range of Ions in Matter (SRIM 2013) software [10] for various incident monochromatic proton energies impinging on different thicknesses of the studied materials. By fitting a Gaussian to the proton distribution, after the protons passed the material foil, the mean proton energy (E_m) and the FWHM were determined for each combination of thickness and initial proton energy. Using the TYpLi code, integral neutron spectra up to 90°, produced by protons with Gaussian distributions, were calculated for each set of E_m and FWHM. A fitting program has been implemented using the TYpLi code with E_m and FWHM as parameters. The fitting procedure adjusted the parameters to better reproduce the theoretical 30 keV Maxwell–Boltzmann distribution. The fitting quality was calculated at each step by the R^2 coefficient. The R^2 coefficient for a data set y_i with n values, means of $\bar{y} = 1/n\sum_i y_i$, and associated predicted value f_i, is defined as:

$$R^2 = 1 - \frac{\sum_{i=1}^{n}(y_i - f_i)^2}{\sum_{i=1}^{n}(y_i - \bar{y})^2}. \tag{4}$$

The R^2 values closer to 1 mean calculated neutron spectra with better fits to the Maxwellian distribution.

One of the isotopes of titanium has a low energy threshold value ($E_p = 1.41$ MeV) for neutron production. For this reason, Ti was rejected as a shaper candidate material because neutrons from lower proton energies could be present even with an isotopic abundance as low as 5%. Carbon is a good candidate since the reaction ^{12}C(p,n)^{12}N has 19 MeV as the proton energy threshold for neutron production, with ^{12}C natural abundance of 99%. To produce an MBNS with $kT = 30$ keV with a single carbon layer, the required proton energy is higher than the threshold for neutron production in ^{13}C. Besides, the needed proton energy is beyond the limits of the accelerator employed in the

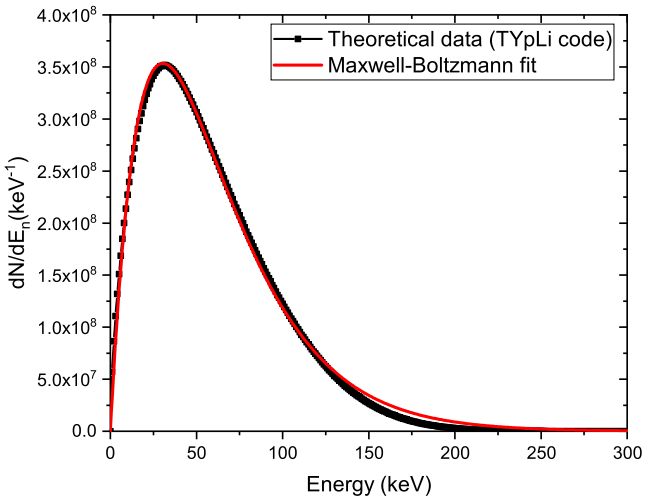

Fig. 2. Model calculated (TYpLi code) neutron energy spectrum integrated from 0° to 90°, for initial proton energies E_p = 3.17 MeV and an aluminum foil of 50 μm thickness.

experiment. For these reasons, carbon was also discarded. Different combinations of proton energies (E_p) and thickness for a foil of copper were also studied. The reaction ^{65}Cu(p,n)^{65}Zn has a proton energy threshold of 2.17 MeV for neutron production. It was impossible to find a combination of E_p and copper thickness that generates an MBNS with kT of 30 keV for proton energies lower than 2.17 MeV. Combinations of layers of different materials were also considered. Even though multiple layers could produce a better MBNS at 30 keV, a single-layer material was chosen because it simplifies the shaper construction. Lead and aluminum are good choices since both materials have a high energy threshold for neutron production. The calculations performed with SRIM on lead showed that a slight variation in the foil thickness drastically modified the produced neutron spectrum. Available lead foils typically have 20%–25% tolerance in their thickness. The above considerations led us to choose aluminum as the material for the proton energy shaper. A proton energy E_p = 3.17 MeV and a thickness of 50 μm were obtained using the aforementioned procedure. These values produced the best coefficient of determination R^2 between the generated neutron spectrum and the 30 keV Maxwell–Boltzmann distribution.

These conditions produced a proton energy distribution with E_m = 1.9094 MeV and FWHM = 0.0937 MeV. According to calculations, the interaction of this proton beam on a thick lithium target produces the neutron spectrum shown in Fig. 2. The fit to a Maxwell–Boltzmann distribution is also shown in the figure. A thermal temperature of 30.18 ± 0.08 keV was obtained from this fit, with R^2 = 0.997.

3. Determination of the experimental neutron spectrum

In neutron time-of-flight (nTOF) experiments, the neutron energy is determined from the time it takes to travel a specified distance (flight path). The precise knowledge of the neutron time and energy relation is essential when the nTOF technique is employed.

Contrary to the idealized one-to-one correspondence between nTOF and neutron energy, the neutron flight time for a single energy varies due to different flight paths between the producing target and the detection position in the detector volume. Additionally, multiple scattering and moderation may occur. Hence, when a single neutron energy is sampled, the resulting TOF is a distribution. The neutron TOF spectrum is converted to an energy spectrum by convolution in the form of a matrix:

$$T_i = \sum_{j=1}^{n} RM_{ij} \times E_j^{emitted} \quad i = 1...n, \tag{5}$$

or in vector form:

$$\mathbf{T} = \mathbf{RM} \times \mathbf{E_e}, \tag{6}$$

where $\mathbf{T}$ is the nTOF spectrum, $\mathbf{RM}$ is the convolution matrix (or response matrix), and $\mathbf{E_e}$ is the (yet unknown) neutron energy spectrum. In the nTOF spectrum, the scored T_i for the ith time bin is composed by tallying the components of the emitted energy spectrum $E_j^{emitted}$ multiplied by a factor equal to the contribution of the jth energy interval to the ith time bin. This factor is the corresponding element RM_{ij} of the response matrix $\mathbf{RM}$. The emitted neutron spectrum is obtained with the solution of the system of n equations by multiplying the folded TOF spectrum by the inverse of the response matrix:

$$\mathbf{E_e} = \mathbf{RM}^{-1} \times \mathbf{T}, \tag{7}$$

where $\mathbf{RM}^{-1}$ is the inverse of the $\mathbf{RM}$.

The response matrix is characteristic of each experimental setup since it depends on the geometry, the detectors, the neutron's flight path, the experimental area, and the properties of the neutron source. The response matrix cannot be measured directly, and it is commonly evaluated by Monte Carlo simulations. The conversion method relies on the response matrix, hence the importance of precisely knowing the geometry and materials of the detector. In the present work, the $\mathbf{RM}$ was calculated using the Monte Carlo N Particle (MCNPX) [11] simulation code. Detector geometry and material compositions were included in the simulations. The complete $\mathbf{RM}$ determination procedure for this work is reported in Ref. [12,13].

Once the $\mathbf{RM}$ was obtained, the inverted matrix was calculated, the deconvolution method was applied, and the neutron energy spectrum was determined. This conversion method determines the emitted neutron energy spectrum from the TOF spectrum by considering the mean moderation time in the detector, its distribution over time, and the detector's efficiency. With a system of n equations and n variables, the deconvolution of the temporal spectrum is performed, and the energy spectrum is found with a unique solution of this system. Since the matrix elements have been calculated per incoming neutrons, the overall efficiency is directly considered in the matrix.

4. Experiment

The experiment used the CN accelerator at the Laboratori Nazionali di Legnaro (LNL-INFN), Padua, Italy [14]. The accelerator was used in pulsed beam mode (with 600 kHz repetition rate, and 4 ns pulse width), and the experimental setup was placed at the end of the horizontal zero degrees beamline.

4.1. Lithium target

All measurements were performed with metallic lithium (Li) targets of about 100 μm thickness each. Two Li targets were produced for the experiment (Fig. 3, upper). One was used for the calibration of the accelerator (Section 4.3). The second one was used for the Maxwell–Boltzmann neutron spectrum measurement (Section 4.4).

The target assembly (Fig. 3, lower) was composed of a copper backing in which the Li is deposited, a PVC tube to isolate the target and place the Al foil, and a collimator made of two tantalum foils with 5 mm diameter aperture. The copper backing had a hemispherical shape, 14.5 cm radius, with 300 μm thickness to have a negligible perturbation of the produced neutron spectra.

To prevent lithium oxidation the target was kept under an argon atmosphere or in vacuum. The target was cooled by applying an air flow to its external face. A 10^{-6} mbar vacuum level was kept at the target position during the experiment. The Cu backing, the PVC tube, and the collimator were electrically isolated, so the current from the target and the collimator were directly acquired and registered every second.

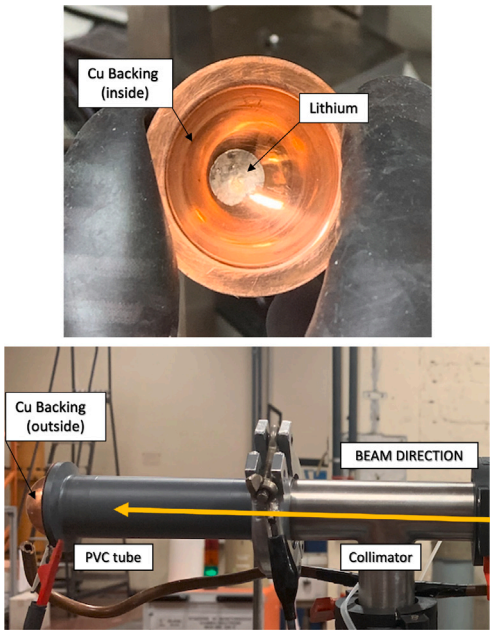

Fig. 3. (Upper) Lithium target, composed by the copper backing and inside the metallic Li. (Lower) Li target assembly at the end of the beamline, composed of a removable Cu backing, an isolated PVC tube and place the Al foil, and a collimator.

Table 1
List of materials and densities in the Li-glass detector. ^{6}Li enrichment is 96%.

Component	Chemical composition	Density (g/cm^3)
Aluminum	Al alloy	2.69
Teflon	$(C_2F_4)_n$	2.20
Glass	SiO_2 56%, MgO 4%, Ce_2O_3 4%, Al_2O_3 18%, $^6Li_2O$ 18%	2.60
Optical RTV	H 8.2%, C 32.4%, 21.6%, Si 37.8%	1.03
Quartz	SiO_2	2.65
μ-metal	C 0.02%, Mn 0.50%, Si 0.35%, Ni 80.00%, Fe 14.93%, Mo 4.20%	8.74
Glass fiber tape	SiO_2 56.0%, ZrO_2 14.5%, B_2O_3 8.0%, AL_2O_3 5.5%, F_2 5.0%, TiO_2 6.0%, Fe_2O_3 5.0%	1.00
Epoxy	$C_{18}H_{21}ClO_3$	1.20

4.2. Detectors

Lithium-glass detectors are widely employed in applications where timing is crucial since they offer the advantage of being relatively fast scintillators and handling reasonably high count rates. Three ^{6}Li-glass detectors of two-inch diameter were purchased from Scionix [15]. Two one-inch thick detectors and one half-inch thick were employed. A fourth, 3 mm thick Li-glass detector was also used as a neutron counter monitor for spectra normalization at different angles.

The geometry of the detector and its material composition were provided by the manufacturing company (Scionix). Furthermore, the characteristics of the optical interface (Quartz) from the PMT (model ETL9214QKB) were provided by the company ET Enterprise [16]. The detector layout and chemical composition employed in the MCNPX simulations (for the response matrix calculation) are shown in Fig. 4 and Table 1, respectively.

4.3. Proton time-of-flight spectrometry and accelerator calibration

The time-of-flight spectrometry of the proton pulsed beam (pTOF) was implemented to determine the proton beam energy and its distribution. Two identical capacitive pickups were inserted in the horizontal beamline to detect the passage of the proton bunch at a distance of about 9.8 m. The time difference (t) between the signals from the two capacitive pickups was measured and corrected for the cables and electronics delay time. A CAEN DT5751 digitizer recorded signals from the pickups, and the time the beam passed through was determined by the zero crossing of the signal. The proton kinetic energy was calculated from Eq. (8),

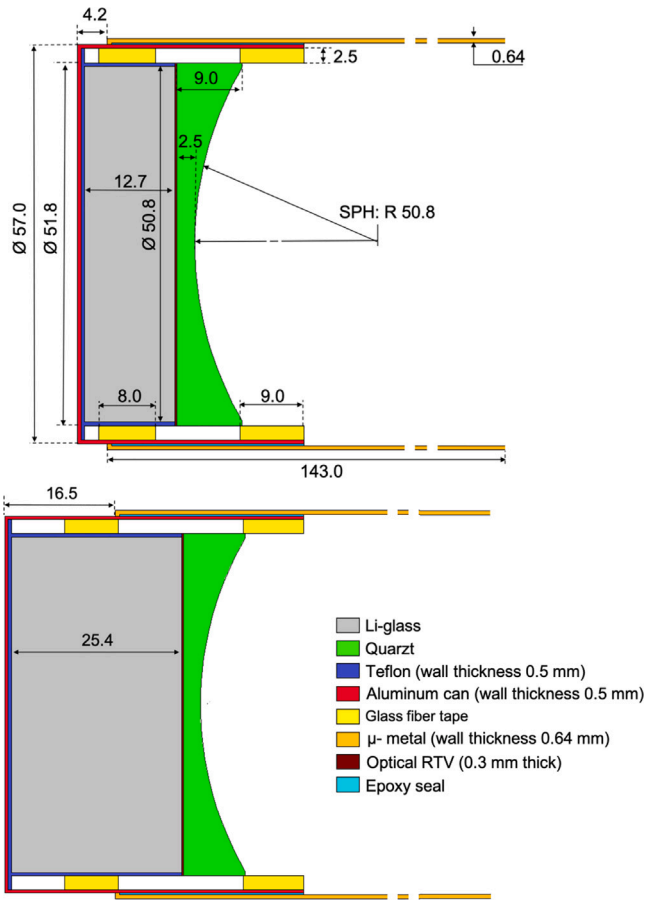

Fig. 4. Layout of the Li-glass detectors: (Upper) Half-inch thick glass detector; (Lower) One-inch thick glass detector. All quantities are in millimeters.

$$E_p = M_p c^2 \left[\frac{1}{\sqrt{1 - \left(\frac{x}{ct}\right)^2}} - 1 \right], \tag{8}$$

where $M_p c^2$ is the proton mass at rest, c is the speed of light, and t is the time for the protons to travel the distance x.

The presence of focusing magnets and lenses in the beamline can modify the proton beam trajectory (proton flight path), so the distance x is not necessarily the geometrical distance between the capacitive pickups. To properly determine the flight path x, the accelerator was calibrated by scanning the ^{7}Li(p,n)^{7}Be reaction near its threshold. This procedure is well described in the work of Martín-Hernández [17].

4.4. Experimental setup

The proton beam energy was set to 3170 keV using the time-of-flight spectrometry of the proton pulsed beam (pTOF). As a proton energy shaper, the 50 μm thick aluminum (Al) foil was placed just before the lithium target, and a pulsed proton beam of 600 kHz repetition rate and approximately 4 ns time width (FWHM) was used. The measured average current on target was around 100 nA during the experiment.

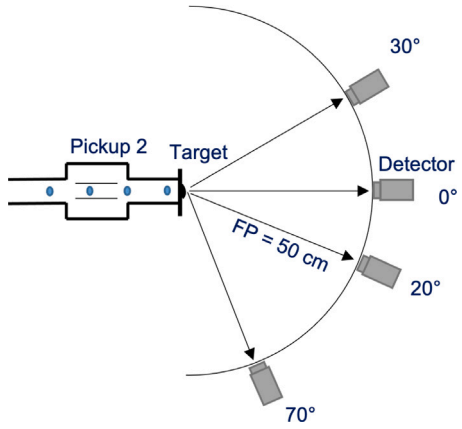

Fig. 5. Schematic representation of the experimental setup. Detectors were located 50 cm from the target at different angles to measure the neutron time-of-flight.

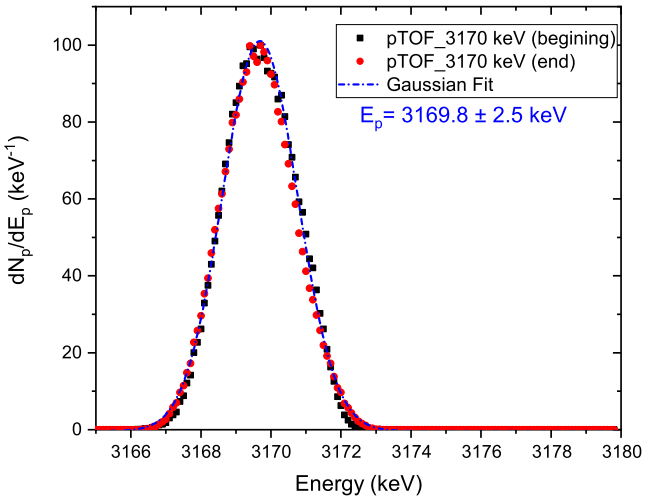

Fig. 6. Proton energy distribution with a mean energy of 3169.8 keV and an FWHM of 2.5 keV, determined with proton time-of-flight (pTOF) spectrometry.

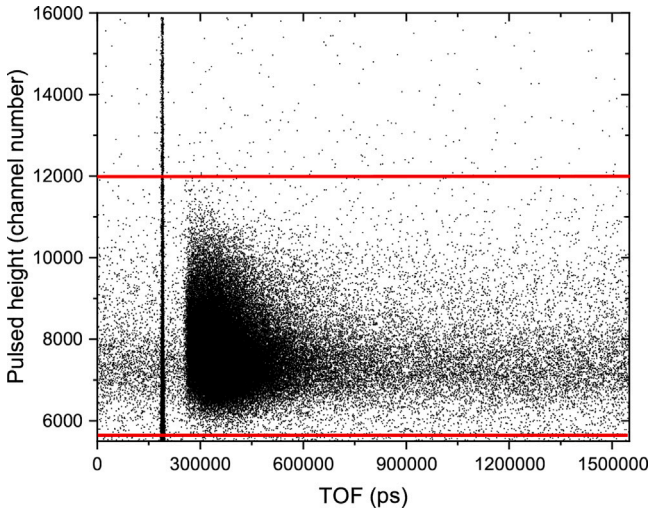

Fig. 7. Two-dimensional plot that shows the detector Pulse height *vs* Time-of-flight (TOF), for the one-inch detector at 20° angle position.

The schematic representation of the experimental setup is shown in Fig. 5. A low-mass goniometer was designed and constructed of carbon fiber and aluminum with movable stands for placing the detectors. It was carefully aligned with the beam pipe and positioned using a laser about 20 m downstream of the target position.

Four Li-glass detectors were simultaneously employed to measure different angles and to improve the statistics. The target-detectors' distances were 49.97±0.01 cm in the same plane as the proton beam and the target, parallel to the floor. This flight path and the selected repetition rate allowed us to measure neutron energy down to 1 keV and prevented the overlapping of neutrons from different proton bunches. The 3 mm thick Li-glass detector was always kept at zero degrees as a neutron monitor. This monitor was used for spectrum normalization, scaling each spectrum by the monitor neutron counts. It was also employed to monitor the beam and the target stability throughout the experiment. Spectra were acquired in 10° steps, from 10 to 90 degrees, with each of the other three detectors, described in Section 4.2. For data acquisition, a CAEN DT5730SB digitizer was used and controlled by the CoMPASS software [18].

5. Results and discussion

5.1. Proton time-of-flight spectrometry

A mean proton energy of 3170 keV was set with proton time-of-flight spectrometry (pTOF) (See Section 4.3). Using Eq. (8), the proton energy distribution was determined, employing as parameters the proton flight path, the TOF distribution of protons, the speed of light and the proton rest mass. The resulting proton energy distribution measured with pTOF is shown in Fig. 6. Two plots are included in the figure. The first refers to the measurement's beginning before measuring the nTOF spectrum. The second one was acquired at the end of the nTOF measurement. In this way, the stability of the accelerator was crosschecked. The figure illustrates the stability of the proton beam; the proton distribution remained the same for the duration of the measurement, ensuring that the emitted neutron spectrum is a product of the same proton beam. A mean proton energy of 3169.8 keV with a full width at half maximum (FWHM) of 2.5 keV was obtained by fitting a Gaussian to the distributions.

5.2. Neutron spectrum analysis

In the nTOF spectrum measurement, the goniometer allowed the movement of the three Li-glass detectors around to measure different angles, from 10° to 90°, in steps of 10°. The fourth Li-glass detector, used as a neutron monitor, was kept at zero degrees. A coincidence window of 1.66 μs (1/600 kHz) was set in the CoMPASS software. The coincidence of the signals of each detector with the signal of the capacitive pickup (the closest to the target) was acquired and saved for post-processing data analysis. FPGA was used to get zero dead time even with a such high trigger rate.

In the online analysis, an energy cut around the neutron peak in the detector pulse height spectra was applied in the software window, thereby eliminating most of the stray gamma events and thus reducing the count rate. As an example, Fig. 7 shows the two-dimensional plot Pulse height *vs* TOF for the one-inch detector at 20° angle position. In the figure, each black point represents a detected particle (neutron or gamma). For better visualization, only 1000000 events are shown in the figure. The vertical pattern, almost a line, is the γ rays arriving first in time since they travel with the speed of light. The neutrons are the horizontal band pattern that covers higher times. The remaining stray events (background) are not correlated neutrons with the capacitive pickup signal or γ rays that have pulse heights inside the neutron energy window.

In offline data analysis another cut in pulse height was applied, represented in Fig. 7 as the region between the two horizontal red lines. Forward analysis included the projection on the TOF axe to obtain the

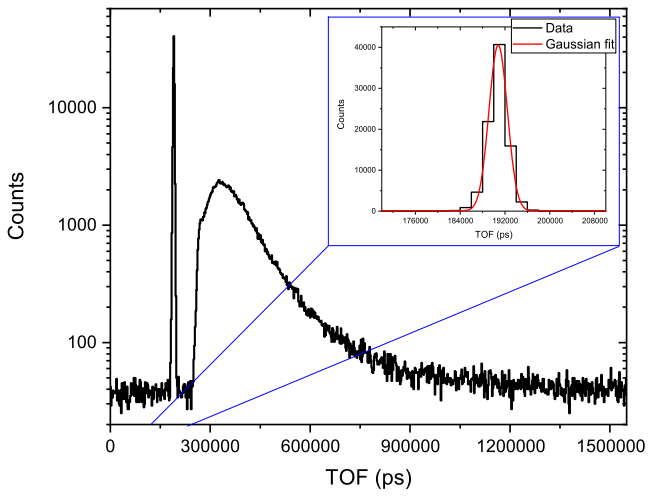

Fig. 8. Time-of-flight histogram at 20° angle position, measured with one-inch thickness Li-glass detector 50 cm from the target.

TOF histogram and an analysis of the gamma flash peak. The obtained TOF histogram is shown in Fig. 8, for the one-inch detector at 20°. The neutrons are well discriminated from the prompt γ peak, ensured by the 50 cm detector flight path. The level for the neutron background was estimated at each angular detector position by determining the average background in the regions between the γ flash and the fastest neutrons, and at very low TOF (before the γ flash peak). The background level for each angle was always flat and, within the statistics, it had the same value (when normalized to monitor). This fact indicates that the background at each angle is not correlated with the TOF and that a constant value can be subtracted from the neutron TOF spectrum. The value of the background was subtracted in the neutron TOF spectrum for each angle detector position. In the figure, the γ flash histogram is also zoomed in. The γ flash represents the time of the proton pulses and gives the measurement of the proton pulse width (time resolution of the beam). In general, the FWHM of the Gaussian fit of the gamma flash distribution was less than 4 ns, in Fig. 8 is 3.43 ± 0.05 ns ($\sigma = 1.46 \pm 0.02$ ns). In the MCNPX simulation, the source was sampled as a Gaussian-shaped time-dependent distribution to mimic the beam time structure.

Different glass thicknesses in the detectors have different **RM**. Because of this, two separate analyses were done, one for the half-inch-thick detector and the other for the one-inch-thick detectors. Since both one-inch detectors are equal, a final spectrum was obtained from the sum of the neutron spectrum counts, thus improving the statistics of the measurement.

For the integrated neutron spectrum, a solid angle correction must be included in the calculation of each angle spectrum. This correction depends on the flight path between the detector and the target and the angle where the detector is placed. The flight path was the same for each angle detector position. The neutron spectrum was measured in steps of 10° and each detector covered approximately an angle of 6°. Employing the equation of the solid angle of a cone with 2θ angle aperture, $\Omega = 2\pi(1 - \cos\theta)$, the scaling factor is proportional to the revolution area of the detector around the axis from the center of the target to the center of the detector at zero degrees. The solid-angle factor was calculated as:

$$f_\alpha = \frac{\Omega_2}{\Omega_1} = \frac{2\pi[1-\cos(\alpha+5°)] - 2\pi[1-\cos(\alpha-5°)]}{2\pi(1-\cos 3°)} = \frac{\cos(\alpha-5°) - \cos(\alpha+5°)}{1-\cos 3°} \quad (9)$$

where Ω_1 is the solid angle subtended by the detector, and Ω_2 is the difference of solid angles between two cones with angles $\alpha + 5°$ and $\alpha - 5°$. Table 2 shows the values obtained for the correction factor.

Table 2
Solid-angle correction factors. Values were normalized to the maxima. Each measured nTOF spectrum was multiplied by the corresponding factor.

Angle	10°	20°	30°	40°	50°	60°	70°	80°	90°
f_α	0.20	0.35	0.51	0.65	0.78	0.88	0.95	1.00	0.51

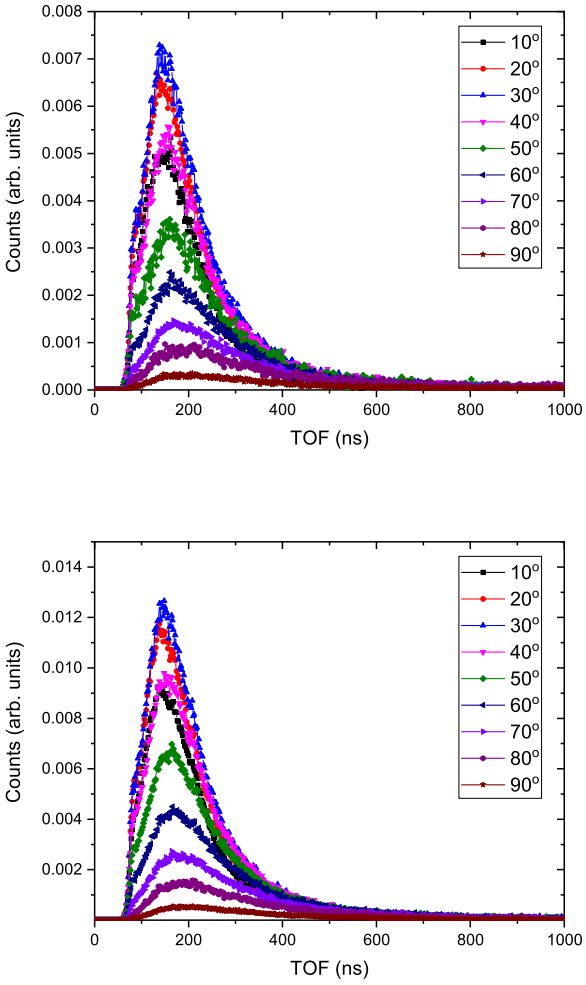

Fig. 9. Angular neutron time-of-flight (TOF) spectra acquired with (Upper) half-inch, (Lower) one-inch thick ^{6}Li-glass detectors over a flight path of 50 cm, from 10 to 90 degrees in steps of 10 degrees, with a proton energy of 3170 keV and the aluminum foil as proton beam shaper. Spectra are already normalized to the monitor counts and corrected for the solid-angle factor.

The final neutron TOF spectrum for each angle (from 10° to 90°) is shown in Fig. 9. Each spectrum was corrected by the solid-angle factor and normalized to the neutron monitor counts.

Applying the method of Section 3, each measured spectrum from Fig. 9 was converted to an energy spectrum by employing the respective response matrix for the Li-glass detector. The time bins were chosen to have almost the same counting statistic per bin, with about 1% statistical uncertainty. Fig. 10 shows the neutron energy spectra per angle obtained with (upper) half-inch and (lower) one-inch thick Li-glass detectors after the conversion method employing the measured nTOF spectrum (Fig. 9).

5.3. Angle-integrated energy spectrum

The 0°-90° angle-integrated nTOF spectrum was determined by summing the TOF spectra from Fig. 9, obtained from the experiment

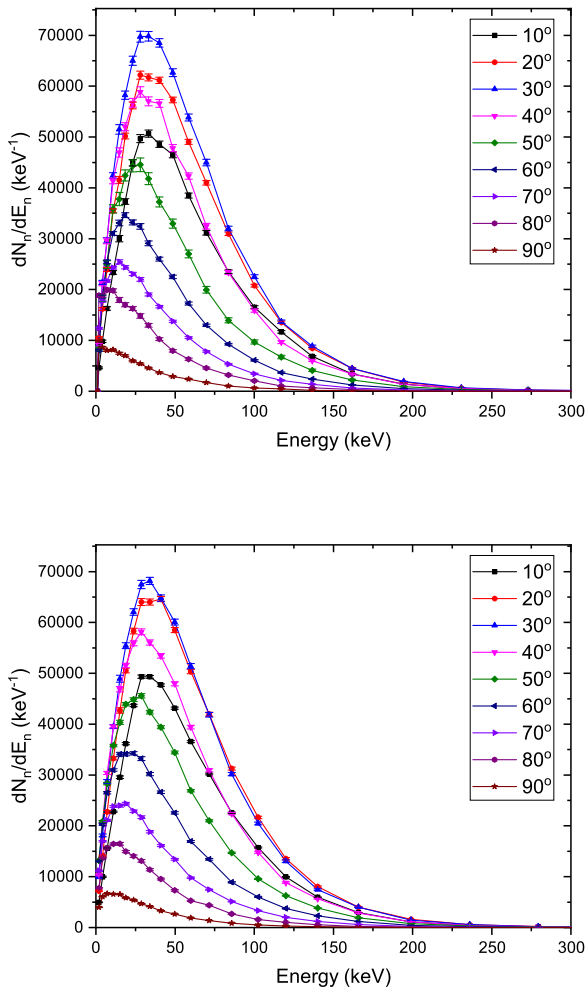

Fig. 10. Neutron energy spectra per angle with (Upper) half-inch, (Lower) one-inch thick Li-glass detector, from 10 to 90 degrees in steps of 10 degrees, measured with proton energy of 3170 keV and the aluminum foil as proton beam shaper. Spectra are already normalized to the monitor counts and corrected for the solid-angle factor. Uncertainties are statistical.

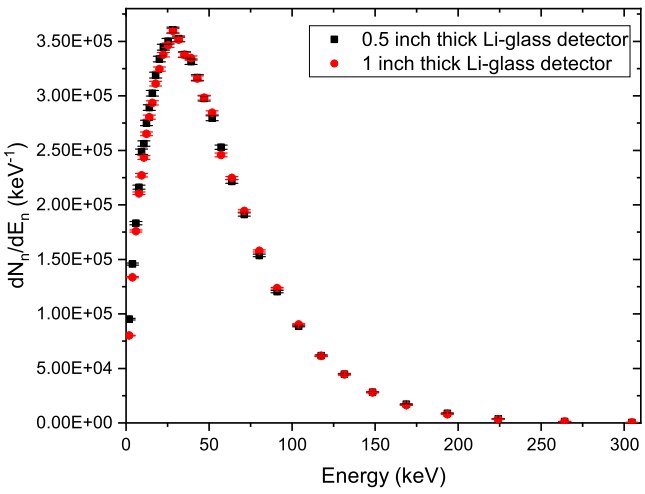

Fig. 11. 0°-90° Angle-integrated neutron energy spectrum for proton energies of 3170 keV and the aluminum foil as proton beam shaper. Uncertainties are statistical.

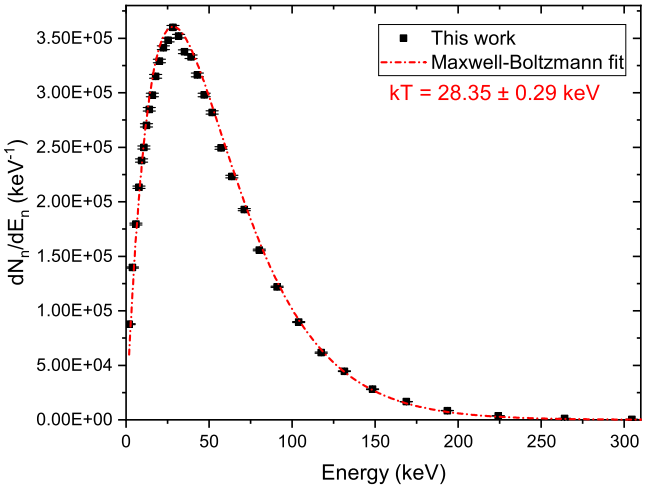

Fig. 12. Final angle-integrated, from 0° to 90°, neutron energy spectrum and the Maxwell–Boltzmann least squares fit. Uncertainties are statistical.

with the one-inch and half-inch thick Li-glass detectors. For each detector type, the spectrum was converted using the previously described **RM** (Section 3). The resulting angle-integrated neutron energy spectrum is shown in Fig. 11. As seen in the figure, the agreement between these spectra is quite good. This measurement was performed with two different detectors, and it is essential to highlight that the same neutron spectrum was obtained, as expected.

5.4. Discussion of uncertainties

As already mentioned, for converting the TOF spectrum to an energy spectrum, the time bins were chosen to have almost the same counting statistic per bin, about 1% statistical uncertainty. The statistical uncertainty on each spectrum of Fig. 10 was less than 5%, except in the high energy part where the counting statistics were low (E_n > 100 keV statistical uncertainties < 15%).

Since Fig. 11 accounts for all the statistics for each detector type, the statistical uncertainty on each neutron energy spectrum was less than 2%. The acquired statistics made it possible to obtain the neutron energy spectrum with 34 nonlinear energy bins, from 1 keV to 322 keV. The higher part of the energy spectrum was obtained using 4 ns temporal bins, limited by the time resolution of the measurement. At lower energies, the spectrum was obtained with energy bins of 2 keV. The energy resolution goes from 2.6% at 1.85 keV to 28.1% at 300 keV.

Systematic uncertainties arise mainly due to the knowledge of the reaction cross sections involved in the neutron interactions in the detector. They were estimated by the propagation of uncertainty on the neutron detection probability as a function of energy, which can be approximated as the ratio of the macroscopic ^{6}Li(n,t)^{4}He cross section to the macroscopic total cross section of the Li-glass. The latter is mainly formed by the scintillator constituents' elastic scattering cross section. In the energy range from 2 keV up to 20 keV, a 0.9% uncertainty was calculated, while from 20 keV up to 250 keV, the averaged uncertainty is 2%, with peak values of 3%, 5%, and 7% in some energy intervals. This is due to the presence of wide resonances in the elastic scattering of some elements present in the scintillator. The uncertainties discussed above are summarized in Table 3.

5.5. Maxwell–Boltzmann neutron spectrum

The final neutron energy spectrum obtained for the MBNS measurement is shown in Fig. 12. It was calculated as the average of the values for each energy bin in Fig. 11. The least squares fit to a Maxwell–Boltzmann distribution is also represented in the figure. The equation of this distribution is:

$$f(E) = \frac{d\mathrm{N}}{dE} = a \cdot E \cdot \exp\left(\frac{-E}{kT}\right), \tag{10}$$

Table 3
Statistical and systematic uncertainties.

Statistical uncertainties	Value	
	E_n < 100 keV	100 keV≤ E_n ≤ 322 keV
Neutron energy spectra per angle (Fig. 10)		
One-inch detector	< 3%	< 8%
Half-inch detector	< 5%	< 15%
0°-90° Angle-integrated neutron energy spectrum (Fig. 11)		
One-inch detector	< 0.6%	< 1%
Half-inch detector	< 1%	< 2%
Maxwell–Boltzmann neutron spectrum (Fig. 12)	< 0.6%	< 1%

Systematic uncertainties	Value
2 keV≤ E_n < 20 keV	0.9%
20 keV≤ E_n ≤ 322 keV	2%

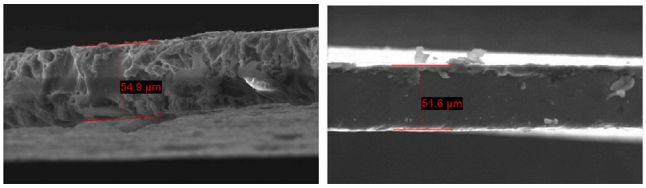

Fig. 13. Image of the thickness of the aluminum foil, taken on a scanning electron microscope (SEM), (Left) edge of the rectangular portion of the foil after electro-erosion processing, (Right) original edge of the aluminum rectangle as cut by Goodfellow company.

where a is a parameter that reflects the maximum value of the $f(E)$ distribution, and kT is the thermal temperature of the distribution (second parameter). The parameter values resulting from the fit are $a = (3.46 \pm 0.08) \times 10^4$ n/keV and $kT = 28.35 \pm 0.29$ keV. As seen in the figure, there is a good agreement between the experimental data and the Maxwell–Boltzmann fit, even in the high energy part of the spectrum, which the R&K work fails to reproduce.

With the proton energy of 3169.8 ± 2.5 keV and the aluminum foil of 50 µm thickness, the obtained MBNS did not have the expected 30 keV thermal temperature. Since the accelerator was calibrated, the discrepancy likely arises from an error in the thickness of the aluminum foil.

A study of the thickness of the Al foil was performed with a scanning electron microscope (SEM). A small rectangular portion of the original aluminum foil supplied by the Goodfellow Company [19] was prepared for the thickness analysis by cutting two sides of the rectangle with an electro-erosion machine, and leaving the other two sides as cut by the supplier. Results of SEM analysis of both types of edges are shown in Fig. 13. The following values were found: 55.85 ± 1.8 µm for the electro-erosion-cut edges and 51.80 ± 3.1 µm for the Goodfellow-cut edges.

This measurement shows the uncertainty in the thickness estimation of the Al foil. The nominal thickness value reported by the Goodfellow company is 50 µm ± 15%, meaning 50.0 ± 7.5 µm. Both measurements performed with the SEM analysis are within the uncertainty reported by the Goodfellow company. The following calculations were performed to have a crosscheck estimation of the real thickness. With the SRIM 2013 software, the distributions of protons after passing different thicknesses of the aluminum foil (50–55 µm) were calculated. An initial proton energy of 3169.77 keV was considered. With each Gaussian distribution's mean value and FWHM, the theoretical neutron spectrum was calculated with the TYpLi code (reported in Section 2). Then, each generated spectrum was compared with the experimental one, and the R^2 coefficient was determined (Fig. 14). As a result, with the best fit

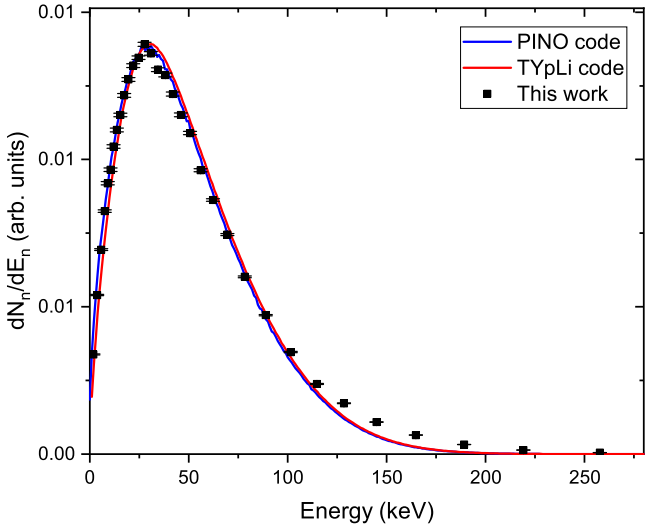

Fig. 14. Angle-integrated neutron energy spectrum obtained in this work compared to the calculations made with the TYpLi and PINO codes.

(highest R^2 value), the aluminum foil thickness was found to be 51 µm. The difference between the expected 30 keV stellar temperature value and the obtained $kT = 28.35 \pm 0.29$ keV could be due to the difference between the estimated thickness and the real one, including thickness inhomogeneity. The theoretical neutron spectrum obtained with the TYpLi code for $E_p = 3169.77$ keV and the estimated 51 µm aluminum foil is shown in Fig. 14. The theoretical neutron spectrum obtained with the PINO code [20] is also shown in the figure. Both code calculations are in very good agreement with the experimental data.

The experimental neutron energy spectrum was also compared with the ones reported in the work of Feinberg et al. [4], shown in Fig. 15. The experimental data from this work was taken from the Experimental Nuclear Reaction Data (EXFOR) [21]. The MBNS obtained in this work reproduces the ideal stellar spectrum better over the entire range, especially in the higher energy region where the other work fails.

6. Conclusions

In this work, neutron time-of-flight spectrometry (nTOF) was applied to determine the neutron spectrum. As the source of neutrons, the ^{7}Li(p,n)^{7}Be nuclear reaction was employed, using a metallic lithium target and a 600 kHz proton pulsed beam from the Van de Graaff accelerator of the Laboratori Nazionali di Legnaro (LNL-INFN), in Padua, Italy.

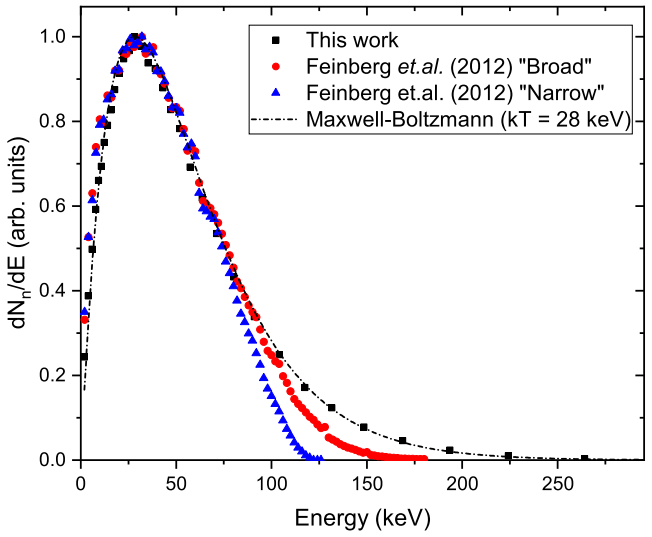

Fig. 15. Neutron energy spectrum obtained in this work compared with Feinberg's work [4] and the Maxwell–Boltzmann least squares fit.

To produce a Maxwell–Boltzmann neutron spectrum (MBNS) with a desired kT, the method of using a proton energy shaper was employed. The experiment was performed with an initial proton energy of 3170 keV and an aluminum foil of 51 μm thickness. To obtain the Maxwellian Averaged Cross Section (MACS) from an activation measurement, the neutron spectrum should correspond to the thermal spectrum in the stars. The most important achievement of this work is that a well-reproduced MBNS with a thermal temperature of 28 keV was measured. Setting the same proton energy and employing the same aluminum foil, the $kT = 28$ keV MACS measurements for different isotopes will be measured in future experiments.

CRediT authorship contribution statement

Elizabeth Musacchio-González: Writing – review & editing, Writing – original draft, Visualization, Validation, Software, Methodology, Investigation, Formal analysis, Data curation, Conceptualization. **Pierfrancesco Mastinu:** Writing – review & editing, Visualization, Validation, Supervision, Project administration, Methodology, Investigation, Data curation, Conceptualization. **Guido Martín-Hernández:** Writing – review & editing, Visualization, Methodology, Conceptualization. **Ignacio Porras:** Writing – review & editing, Methodology. **Lisa Centofante:** Writing – review & editing, Investigation. **Fernando Arias de Saavedra:** Writing – review & editing, Methodology. **Luca Maran:** Investigation. **Alberto Ruzzon:** Investigation, Data curation. **Daniele Lideo:** Investigation.

Declaration of competing interest

The authors declare that they have no known competing financial interests or personal relationships that could have appeared to influence the work reported in this paper.

Data availability

Data will be made available on request.

Acknowledgments

This work has been supported by the SPARE (Space Radiation Shielding) project: a joint INFN, ASI, and Centro Fermi collaboration. We would like to thank the CN accelerator technicians for their support, good beam conditions, and continuous help during the experiment.

References

[1] W. Ratynski, F. Käppeler, Neutron capture cross section of Au197: A standard for stellar nucleosynthesis, Phys. Rev. C 37 (2) (1988) 595–604, http://dx.doi.org/10.1103/PhysRevC.37.595.
[2] R. Reifarth, P. Philipp Erbacher, Fiebiger, K. Göbel, T. Heftrich, M. Heil, F. Käppeler, N. Klapper, D. Kurtulgil, C. Langer, L.-W. C., A. Mengoni, T. B., S. Schmidt, M. Weigand, M. Wiescher, Neutron-induced cross sections, Eur. Phys. J. Plus 133 (424) (2018) http://dx.doi.org/10.1140/epjp/i2018-12295-3.
[3] C. Lederer, F. Käppeler, M. Mosconi, R. Nolte, M. Heil, R. Reifarth, S. Schmidt, I. Dillmann, U. Giesen, A. Mengoni, A. Wallner, Definition of a standard neutron field with the 7Li(p,n)7Be reaction, Phys. Rev. C - Nucl. Phys. 85 (5) (2012) 1–8, http://dx.doi.org/10.1103/PhysRevC.85.055809.
[4] G. Feinberg, M. Friedman, A. Krása, A. Shor, Y. Eisen, D. Berkovits, D. Cohen, G. Giorginis, T. Hirsh, M. Paul, A.J. Plompen, E. Tsuk, Quasi-stellar neutrons from the 7Li(p,n)7Be reaction with an energy-broadened proton beam, Phys. Rev. C - Nucl. Phys. 85 (5) (2012) 1–12, http://dx.doi.org/10.1103/PhysRevC.85.055810.
[5] M. Macías, B. Fernández, J. Praena, The first neutron time-of-flight line in Spain: Commissioning and new data for the definition of a neutron standard field, Radiat. Phys. Chem. 168 (2020) 108538, http://dx.doi.org/10.1016/j.radphyschem.2019.108538.
[6] P.F. Mastinu, G. Martín Hernández, J. Praena, A method to obtain a Maxwell-Boltzmann neutron spectrum at kT=30 keV for nuclear astrophysics studies, Nucl. Instrum. Methods Phys. Res., Sect. A 601 (3) (2009) 333–338, http://dx.doi.org/10.1016/j.nima.2009.01.005.
[7] G. Martín-Hernández, P.F. Mastinu, J. Praena, N. Dzysiuk, R. Capote Noy, M. Pignatari, Temperature-tuned Maxwell-Boltzmann neutron spectra for kT ranging from 30 up to 50keV for nuclear astrophysics studies, Appl. Radiat. Isot. 70 (8) (2012) 1583–1589, http://dx.doi.org/10.1016/j.apradiso.2012.05.004.
[8] C.L. Lee, X. Zhou, Thick target neutron yields for the ^{7}Li(p,n)^{7}Be reaction near threshold, Nucl. Instrum. Methods Phys. Res. B 152 (1999) 1–11.
[9] H. Liskien, A. Paulsen, Atomic data and nuclear data tables, 15, (I) 1975, pp. 57–84.
[10] J.F. Ziegler, SRIM - The stopping and range of ions in matter, http://www.srim.org.
[11] D. Pelowitz, MCNPX users manual version 2.7.0, 2011, LA-CP-11-00438.
[12] E. Musacchio-González, P. Mastinu, G. Martín-Hernández, Method for converting neutron time-of-flight spectrum into an energy spectrum, IOP Publ. J. Phys.: Conf. Ser. (2023) in press.
[13] E. Musacchio-González, (Ph.D. thesis), University of Ferrara, 2021.
[14] Legnaro National Laboratories (LNL), https://www.lnl.infn.it/index.php/en/.
[15] SCIONIX- Dedicated scintillation detectors, https://scionix.nl.
[16] ET Enterprises electron tubes, ET Enterprises, Ltd., https://et-enterprises.com.
[17] G. Martín-Hernández, P. Mastinu, E. Musacchio-González, R. Capote, H. Lubián, M. Macías, ^{7}Li(p,n)^{7}be cross section from threshold to 1960 kev and precise measurement of the ^{197}au(n,γ) spectrum-averaged cross section at 30 kev, Phys. Rev. C 99 (3) (2019) 1–10, http://dx.doi.org/10.1103/PhysRevC.99.034616.
[18] CoMPASS multiparametric DAQ software for physics applications, https://www.caen.it/products/compass/.
[19] Goodfellow company, http://www.goodfellow.com.
[20] R. Reifarth, M. Heil, F. Käppeler, R. Plag, PINO—A tool for simulating neutron spectra resulting from the 7Li(p,n) reaction, Nucl. Instrum. Methods Phys. Res. A 608 (1) (2009) 139–143, http://dx.doi.org/10.1016/j.nima.2009.06.046.
[21] Experimental Nuclear Reaction Data (EXFOR) Database Version of 2020-12-19, https://www-nds.iaea.org/exfor/.